Atomic-Scale Spin-Polarized Scanning Tunneling Microscopy and Atomic Force Microscopy: a Review

Arthur R. Smith[*]

Nanoscale and Quantum Phenomena Institute,

Department of Physics and Astronomy,

Ohio University, Athens, OH 45701, USA

Abstract

Atomic-scale spin-polarized scanning tunneling microscopy is a powerful real-space technique for investigating the magnetic structure of surfaces. With its intrinsic lateral resolution capability, this technique can achieve atomic-scale resolved spin resolution of surfaces. Antiferromagnets, in particular, offer opportunities to test the spatial resolution of magnetism at ultimate length scales, where the magnetization reverses on the scale of one atomic spacing. But in addition, the technique has been applied with very interesting results to the case of ferromagnetic surfaces. Reviewed here are the various contemporary experimental results, including a discussion of the theoretical basis for atomic-scale magnetic imaging. Theoretical calculations to simulate the magnetic STM images are also discussed, including those calculations which take into account the tip electronic structure.

---
[*] e-mail: smitha2@ohio.edu

I. INTRODUCTION

Within the last 25 years, great progress has been made in the field of nanometer science and technology. This is due to the invention of the scanning tunneling microscope (STM) by Binnig, Rohrer, and co-workers in 1981, which made possible the ability to actually "see" objects of nanometer size and even down to single atoms.[1] This unique ability to measure materials and devices at such exceedingly small length scales has resulted in astonishing details of materials, previously only imagined. Simultaneous to the development of the field of STM and related scanning probe microscopies (SPM's), many great developments have also occurred in the electronics and magnetism fields. While the field of magnetism is arguably of equal importance as the field of electronics to society, it is amazing to note that within its first 25 years, the STM was mainly used to study the *electronic* structure of surfaces. Only a tiny fraction of STM papers, most of them published within the last 6 years, have described the use of STM for measuring the *magnetic* properties of surfaces.[2–14] In the pages of these papers is found astonishing detail of the nanoscale magnetic structure of ferromagnetic (FM) and antiferromagnetic (aFM) surfaces.

In this Review, it is attempted to gather a large subset (at least) of the important papers in the field of atomic-scale spin-polarized STM (SP-STM). Also discussed is one example of spin-polarized atomic force microscopy (SP-AFM), also referred to as exchange force microscopy. The treatment is primarily restricted to the presentation of those experimental and theoretical works dealing specifically with atomically-resolved SP-STM, or SP-STM in which the measured magnetic signal is directly correlated with atomic or fundamentally periodic structure, e.g. the periodicity of an antiferromagnet whose magnetic structure varies in sync with the orderly atomic structure of the material. First, the basic principle of SP-STM is described and a simple mathematical example given to motivate how the magnetic local density of states is involved in the spin-polarized imaging. Following this begins a sequential discussion of the various experimental results which have been obtained using atomic-scale SP-STM and SP-AFM, including both antiferromagnets and also ferromagnets (1 known case). Following this begins a section on theory, which includes two parts - first, a section dealing with the application of the spin-polarized Tersoff-Hamann formula with a discussion of the theory referred to as star coefficient theory and its applicability to various experimental cases, and second, a section dealing with the inclusion of the STM tip

electronic structure in the calculations. Finally, the paper is briefly summarized with an outlook presented.

II. PRINCIPLE OF SPIN-POLARIZED SCANNING TUNNELING MICROSCOPY

Scanning tunneling microscopy, as is well known, is a powerful method for obtaining real space information about a crystal surface with resolution down to the atomic scale. In normal STM, a conducting sample surface is scanned using a conducting probe tip, and a non-spin-polarized tunneling current flows between the tip and sample. Probe tips commonly used for normal STM are fabricated from platinum-iridium and, more commonly, tungsten. For magnetic samples, however, magnetic contrast can be obtained using magnetic probe tips, and in this case a spin-polarized tunneling current flows between the tip and the sample. Suitable magnetic tip materials include nickel, iron, and CrO2. More recently, magnetically-coated W tips have proven highly successful.[3]

The basic working principle of spin-polarized STM is that, given that tip and sample magnetizations are vectors, the tunneling current will be larger when the vectors are parallel and smaller when they are anti-parallel, with a cosine dependence for in-between orientations. The equation for tunneling current can be written most simply as:[2, 7]

$$I_t \sim \int [1 + P^t P^s cos\theta] dE \tag{1}$$

where P^t and P^s are the spin polarizations of tip and sample, respectively. Variations in the tunneling current, dependent on the sample magnetization orientation, then allows the STM image to become a map of the spin polarization of the sample. This is more fully understood by considering that the tunneling current is actually composed of 2 components - a non-spin-polarized and a spin-polarized component. The spin-polarized component is normally zero in the case of non-magnetic STM tips on non-magnetic surfaces. But it becomes either negative or positive for a magnetic tip on a magnetic surface. In terms of the spin local density of states (LDOS), the tunneling current is written as:[15, 16]

$$I_t \sim \int g_V(E) \frac{1}{2} [n^t n^s + m^t m^s cos\theta] dE \tag{2}$$

where $g_V(E) = f(E\text{-}E_F) - f(E\text{-}E_F\text{-}eV_S)$ with f being the Fermi function and V_S being the applied sample bias; n^t and n^s are the total (spin majority + spin minority) LDOS of tip

3

and sample, and m^t and m^s are the net magnetization (spin majority - spin minority) LDOS of tip and sample, respectively. Therefore, in SP-STM, what is really being measured is a quantity proportional to the convolution-integrated LDOS of sample and tip. It is important to notice that this integral is only over the window of energy defined by the Fermi level and the applied bias between sample and tip. Contrast in the constant current SP-STM image therefore depends on the spin polarization within this energy window between E_F and E_F + eV_S; in dI/dV imaging, magnetic contrast depends on the spin-polarization at E_F + eV_S.

An example of a convolution in the parallel case (Eq. 2) is depicted schematically in Fig. 1(a) in which tip and sample are assumed to have LDOS functions which vary linearly with energy, as depicted, for both spin-↑ and spin-↓. The linear LDOS functions are chosen only for purposes of illustration; they will surely have more complicated functional forms in the case of a real sample and a real tip. We note that for sufficiently small voltages, it is often assumed that the LDOS of the tip is constant with energy over the relevant energy integration window. With that simpler assumption, qualitatively similar results to the example depicted in Fig. 1 and discussed below would be obtained.

In the parallel case, for both sample and tip, the spin-↑ LDOS is majority. Note that both spin-↑ and spin-↓ LDOS are positive values, although the spin-↓ LDOS are plotted on the axis pointing down. In this example, the negative sample bias V_s case is shown; note in this case the relevant sample states are filled while the relevant tip states are empty. For the parallel case, Fig. 1(a) shows that the spin-↑ channel will compose the biggest part of the convolution integral, while the spin-↓ channel will compose the smallest part of the convolution integral. The parabolas shown in Fig. 1 are the integrands of the convolution integrals. The sum of the areas (both positive areas) under the two parabolas is proportional to the total tunneling current. For purposes of the illustration let $n_>^t$(E-eV_s) = 4×(E-eV_s)/eV/atom, $n_<^t$(E-eV_s) = 2×(E-eV_s)/eV/atom, $n_>^s(\vec{R}_t,$E) = -4×E/eV/atom, $n_<^s(\vec{R}_t,$E) = -2×E/eV/atom. Note that all of these quantities are positive values over the energy window between E_F and (E_F + eV_s). Let V_s = -1V. Then applying Eq. 2, the tunneling current $I_{t,max} \sim$ (4×4 + 2×2)($\frac{1}{6}$) = $\frac{20}{6}$ (units of current), for the case of parallel tip and sample spin.

The convolution in the anti-parallel case (Eq. 3) for the same negative sample bias V_s is depicted schematically in Fig. 1(b); here the sample spin-↑ LDOS is minority, while the sample spin-↓ LDOS is majority. In this case, the spin-↑ channel and spin-↓ channel will compose more similar integral values, as indicated by the areas under the parabolas shown
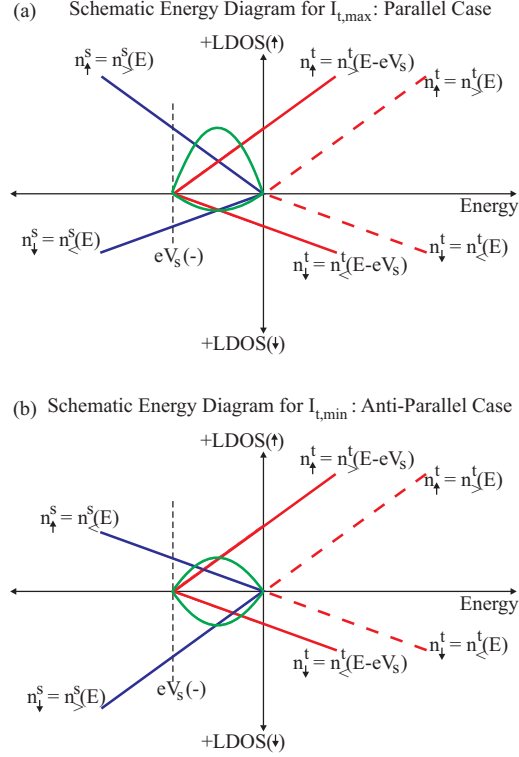
FIG. 1: Schematic energy diagrams of the spin-polarized overlap integrals in the simple case of a sample and tip whose LDOS vary linearly with energy. The sample bias is -1 V. The case in (a) corresponds to parallel tip and sample spins; the case in (b) corresponds to anti-parallel tip and sample spins. Parabolas represent the products of the tip and sample LDOS over the energy range -1 eV to 0 eV.

in Fig. 1(b). Using the LDOS functions given previously and applying Eq. 3, we get that the tunneling current $I_{t,min} \sim (4 \times 2 + 4 \times 2)(\frac{1}{6}) = \frac{16}{6}$ (units of current), for the case of anti-parallel tip and sample spin, which is less than $I_{t,max}$.

This example illustrates that, in the case of a sample in which rows of atoms alternate in their majority and minority spin states (i.e. an antiferromagnet), the tunneling current is modulated as the tip scans across the rows in constant height (CH) mode, and the height of the tip will be modulated as the tip scans across the rows in the case of constant current (CC) mode.

III. ANTIFERROMAGNETIC SPIN STRUCTURE RESOLVED AT THE ATOMIC SCALE

A variety of antiferromagnets have been investigated using SP-STM, including first, single crystal chromium, and later aFM monolayers and thin films. In this section are discussed the published results to date in which SP-STM was used to resolve the antiferromagnet spin structure. The first paper which reported spin resolution on an antiferromagnet also happened to be the paper showing the first experimental SP-STM results. Lastly is discussed a recent report using spin-polarized atomic force microscopy to resolve the aFM spin structure.

III.A. Cr(001) Topological Antiferromagnetism

Wiesendanger *et al.* published the first SP-STM paper in 1990 on the topic of spin-polarized STM imaging of single crystal Cr(001).[2] Interestingly, the Cr(001) surface was predicted to be FM even though its bulk was well-known, from experiment and theory, to be aFM.[17, 18] However, no previous experimental technique had been able to resolve any FM domain structure at the surface of Cr(001). Wiesendanger *et al.* imaged this surface using standard W STM tips, finding a step-terrace morphology with single monolayer steps of height ~ 1.4 Å. Then using CrO_2 tips, a similar morphology was found, except that the step height was found to alternate between 2 values - 1.2 Å and 1.6 Å.

This step height alternation was the first magnetic information ever observed using STM. It was interpreted as being due to the magnetic contribution from spin-polarized tunneling. The step height data was consistent with a surface morphology in which the FM spin direction of a given terrace reversed upon crossing single monolayer steps. Such topological antiferromagnetism had recently been proposed for Cr(001) by Blugel *et al.*[18] In this case then, the STM tip would attain the same tunneling current at 2 characteristic distances from the surface, depending on the terrace. When the terrace magnetization was parallel to that of the tip, the CC tip-sample distance would increase slightly, whereas in the antiparallel case, the CC tip-sample distance would decrease slightly. Then, a step down from parallel to antiparallel would be a larger step, and a step down from antiparallel to parallel would be a smaller step.

Quantitatively, the change in tip-sample distance derived from the step height measurements was 0.10 Å with an error half that amount, whereas the absolute tip-sample distance was determined to be ~ 5 Å. Although this represents only a 2% change in tip-sample spacing, a 0.10 Å change is quite easily measurable in a good STM.

Wiesendanger *et al.* also defined an "effective polarization" P of the tunneling junction and gave an expression for it which depended on the tunneling constant $A \approx 1$ eV$^{-1/2}$ Å^{-1}, the surface work function ϕ, and the measured step height difference from the average $\Delta s = 0.2$ Å. The authors measured ϕ to lie between 3 and 5 eV, concluding that the surface was clean during the measurements. Using the obtained numbers, the effective polarization was derived to be $(20 \pm 10)\%$.

While the results of Wiesendanger *et al.* clearly showed antiferromagnetism of a surface along the z-direction, the required lateral resolution needed was only that corresponding to the average terrace width of the surface and so did not make use of the intrinsic lateral resolution capability of STM. Another limitation of this result was that although the step heights could be easily measured, the magnetic and non-magnetic (topographic) information contained within the whole SP-STM image was superimposed. The ability to decouple these two components would await future developments. Nonetheless, this first published work on SP-STM opened the gates to the important new field of SP-STM research and was the first SP-STM paper on antiferromagnetism.

III.B. A Return to Cr(001): CC- and dI/dV-mode Imaging

Ten years following the initial publication by Wiesendanger *et al.*, Kleiber *et al.* published a new paper on the topic of Cr(001).[8] In this, they showed new results overcoming the limitations of the earlier work. In contrast to the use of CrO_2 tips, they used Fe-coated W tips as previously developed by Bode *et al.*[19] In the new work, two kinds of images were shown, including the CC-mode image of the same step-terrace structure seen in the earlier paper, but also the spectroscopic dI/dV-mode image. Whereas the CC-mode image contains both magnetic and non-magnetic (topographic) contrast between adjacent terraces, the dI/dV-mode image contains only magnetic contrast between adjacent terraces. One then clearly sees the magnetization reversal at the step edges, making use of the lateral resolution of the STM, and that every other terrace has the same magnetization.

In addition to isolating the magnetic information using the dI/dV-mode imaging, Kleiber *et al.* also presented local tunneling spectroscopy results clearly identifying a surface state peak near the Fermi level E_F, whose intensity depended on the relative tip-sample magnetization orientation. Parallel orientation (in constant-separation mode) corresponded to greater peak intensity, whereas anti-parallel orientation corresponded to smaller peak intensity. Kleiber *et al.* explain in detail how that in the CC-mode, the dI/dV spectroscopic image shows the terrace with anti-parallel tip-sample magnetization alignment brighter, while the terrace with parallel orientation is darker. In any case, the terrace-dependent magnetization is clearly resolved.

An additional accomplishment in this paper is the SP-STM imaging of the magnetization in the vicinity of screw dislocations. In this case, domain walls are found, and their width is measured to be   120 nm. Therefore, this is a very gradual change; atomically-abrupt domain walls were found in a different system.

III.C. Atomically Abrupt Domain Walls - Fe on W(110)

One year after the publication by Kleiber *et al.*[8], SP-STM was applied to the case of an ultra-thin transition-metal film - in this case slightly greater than 1 monolayer of Fe on a vicinal W(110) substrate. The vicinal nature of the W(110) substrate led to the formation of narrow Fe nanostripes. Interestingly, although there is no hint of atomic resolution, the dI/dV image clearly reveals the magnetic domains with, remarkably, domain walls having atomic-scale width of only ~ 6 Å. This and other results regarding domain walls near the atomic scale in FM layers are further discussed in another recent publication.[20]

III.D. Antiferromagnetic Mn Monolayer on W(110)

In 2000, Heinze *et al.* impressed the surface magnetism community, not to mention the greater nanoscale magnetism field, with their ground-breaking publication on the spin resolution of a Mn monolayer on W(110) substrate.[7] The non-magnetic (morphological) structure of Mn grown at room-temperature on W(110) was nicely demonstrated in a previous publication by Bode *et al.*[21] In that paper, the authors shows that Mn can be grown on W(110) pseudomorphically up to a local coverage of 3 ML. In their SP-STM experi-

ment, such a pseudomorphic monolayer, grown at substrate temperature $T_{sub} \approx 400$K, was prepared for study.

For the SP-STM study of Mn/W(110), Heinze *et al.* chose to focus on the first Mn monolayer. First principles theory had suggested that this monolayer should have a c(2×2) aFM ground state in which, at some low-enough temperature, the magnetic moments of adjacent nearest neighbor atoms would point in opposite directions.

They imaged this Mn monolayer with 3 kinds of tips: 1) plain W tips, 2) Fe-coated W tips, and 3) Gd-coated W tips. Using the plain W tips, the atomic resolution image of each Mn atom site in 2 dimensions was obtained. This is shown in Fig. 2(a), in which a 27 Å × 22 Å area is resolved. Theory computations were compared with the image, as shown in the inset of Fig. 2(a). As can be seen, the agreement between theory and experiment was shown to be quite good. Next, they applied the Fe-coated W tip to image to Mn monolayer. Bode *et al.* had previously shown that these tips possessed magnetization axes in the plane of the sample.[19] This was considered important since theory suggested that the easy axis should be *in-plane*, and only if the tip and sample magnetization axes have a common vector component is it possible to obtain magnetic contrast. Given such a tip, it might be possible that atomic-resolved images would reveal the spin structure of each atom, a positive or negative signal superimposed on the normal, atomic-resolution image. What they found was completely different.

The image resulting from the use of the Fe-coated W tip is shown in Fig. 2(b). What was completely surprising to the researchers was that, rather than each atomic site having superimposed upon it an enhancement or a depression depending on the spin alignment of sample and tip, the magnetic tip resulted in an image consisting just of stripes running along the [001] direction. This was the case for either the Fe-coated or the Gd-coated W tips. These stripes had a periodicity equal to 2 atomic-row spacings along the [1$\bar{1}$0] direction. All evidence of a non-magnetic signal, as shown with the non-magnetic W tip in Fig. 2(a), had vanished.

It was then discovered that the stripes were exactly what was predicted by first-principles theory, as seen by the theory simulation shown in the inset of Fig. 2(b). This is not unreasonable, considering that every other [001] row consists of atoms with the same spin direction. The magnetic STM imaging therefore resolved the spin of the surface in rows; but in addition, along the [001] row direction, a slight modulation of the row height - predicted
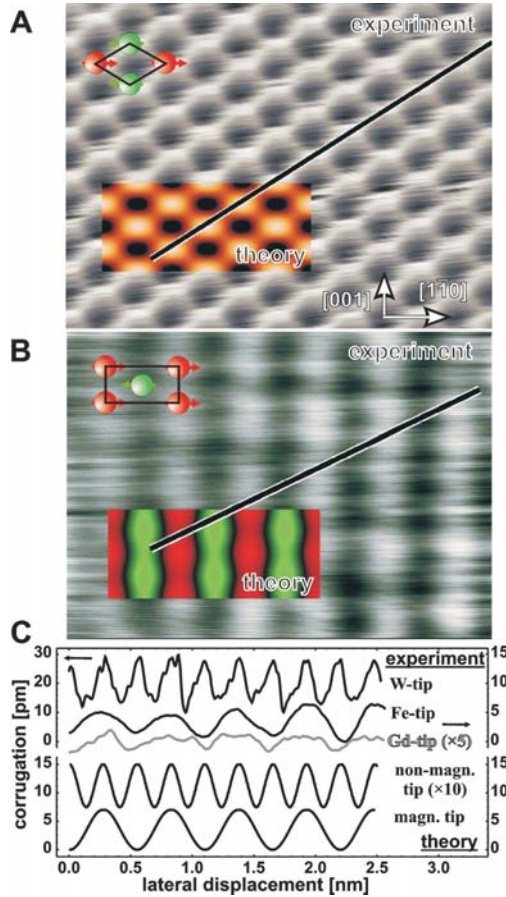
FIG. 2: Comparison of experimental and theoretical STM images of a Mn ML on W(110) with (A) a nonmagnetic W tip and (B) a magnetic Fe tip. (C) Experimental and theoretical line sections for the images in (A) and (B). The unit cell of the calculated magnetic ground-state configuration is shown in (A) and (B) for comparison. Tunneling parameters for both images are I_{tun} = 40 nA and U = -3 mV. The image size is 2.7 nm by 2.2 nm. (Reprinted with permission from S. Heinze, M. Bode, A. Kubetzka, O. Pietzsch, X. Nie, S. Blügel, and R. Wiesendanger, Science **288**, 1805 (2000). Copyright 2000 AAAS.)

by the theory simulation - was apparent.

Still, what was particularly surprising was that the spin-polarized image was entirely magnetic; there was no non-magnetic component. This eliminated the need for any de-coupling of magnetic and non-magnetic information. The application of a magnetic tip resulted in a magnetic image, while the application of a non-magnetic tip resulted in a non-magnetic image. A simple explanation for this contrast behavior can be made in terms of surface

periodicities; it turns out that, in this case, the magnetic tip sees a much bigger response to the magnetic period in comparison with the twice-smaller, atomic period; whereas, the non-magnetic tip only responds to the smaller atomic period. This is explained in more detail in section V.

The paper by Heinze *et al.* was the first convincing demonstration of antiferromagnetism resolved at the atomic scale in the *in-plane* direction. Nonetheless, new and different results waited to be demonstrated in different systems, yielding new insights into the ultimate limits of magnetic imaging.

III.E. Antiferromagnetic Mn_3N_2 (010) Thin Film on MgO(001)

III.E.1 Epitaxial Growth of Mn_3N_2

Two years after the publication of Heinze *et al.*'s Mn ML on W(110) result, observations of spin resolution of an aFM thin film of Mn_3N_2 (010) were published by Yang *et al.*[14] Results from this study provided new compelling evidence for atomic-scale spin-resolved STM while at the same time, presenting additional aspects not seen in the Heinze *et al.* results.

The initial motivation to study manganese nitride sprang from an interest in the widely varying and interesting magnetic properties of the different phases of this material. Up to ca. 2000, manganese nitride had been studied in bulk or thick film form by a number of authors, and much was already known about its phases, stoichiometries, crystal structures, lattice constants, and magnetic properties - which to this day show great promise for future technological applications.[22–31] However, regarding the epitaxial growth of thin films and layers of this material, relatively little if anything was known. And technological applications involving their magnetic and electronic properties would require a sound knowledge of their epitaxial growth.

An additional motivation for studying manganese nitride stemmed from the growing interest in magnetic-doped nitride semiconductors - which began from a single theory paper.[32] In that one paper, Dietl. *et al.* had predicted that Mn-doped GaN (and also ZnO) may be a dilute FM semiconductor at room temperature if the doping concentration, carrier type, and carrier density satisfied certain stated conditions. From this perspective, if a ternary

compound based on manganese nitride and gallium nitride was to become important tech-nologically for the new field referred to as *spintronics*, then it should also be important to fully explore the epitaxial growth of the two binary compounds; moreover, epitaxial growth of GaN was already far advanced.

Smith *et al.* thus began to study manganese nitride in ca. 2000, with the goal to grow thin films using molecular beam epitaxy and study them using STM. The first findings of this study were published by Yang *et al.* in 2001.[33] Under certain Mn-rich growth conditions, an (010)-oriented, aFM Mn_3N_2 thin film grew epitaxially on top of the oxide MgO(001) which was used as substrate. By varying the manganese flux, it was possible to re-orient this film to the (001) orientation during growth. Furthermore, by varying both the manganese flux and the substrate temperature, it was possible to control both the phase and orientation.[34]

Yang *et al.* showed that using a W tip, the STM image of Mn_3N_2 (010) shows a row-like structure within each of two 90°-rotated domains. That row-like structure was shown to correspond perfectly with the (010) termination of the bulk Mn_3N_2 structure. The bulk structure of Mn_3N_2 was known from the work of Jacobs *et al.*, and it consists of a face-centered tetragonal lattice with a 2 atom (Mn and N) basis set; this is the rock-salt type structure.[27] For the (010) surface, the spacing of the rows corresponded to the spacing between planes of nitrogen vacancies in the bulk model - these occur every third atomic layer along the (001) direction. The [001] direction is therefore parallel to the (010) film surface and perpendicular to the [100]-aligned rows seen in the STM image.

Zoom-in images of the Mn_3N_2 (010) surface using ultra-sharp STM tips revealed each Mn atom of the surface. Those along the center of the row appeared bright, while for each bright atom, there were two darker-appearing atoms off-center of the row. The detailed study of the tip-sample bias-dependence of the contrast in these atomic-scale resolved STM images was shown later by Yang *et al.* and compared with theory predictions based on bulk first-principles LDOS calculations by W.R.L. Lambrecht.[35] A good agreement was found between experiment and theory. Lambrecht *et al.* also published a theory paper showing that for both MnN and Mn_3N_2, the Mn-atom LDOS is dominant over N-atom LDOS near the Fermi level;[36] the STM images therefore show only Mn atoms.

III.E.2 Spin Resolution of Mn₃N₂ (010) using SP-STM

In their work (2002), Yang *et al.* used Mn-coated and Fe-coated W tips to image the
Mn$_3$N$_2$ (010) surface.[14] According to the simple bulk picture, every adjacent [100] row of
atoms at the surface should have opposite spin direction. In typical STM images, the row
structure has periodicity of 3 times the simple atomic-row spacing. Therefore, even this 3-by
superstructure should be aFM as understood by the following sequence: ...⇑ ↓ ↑ ⇓ ↑ ↓ ⇑ ↓
↑ ⇓ ↑ ↓ ⇑ ↓ ↑ ⇓ ↑ ↓... Here, the double arrows just denote those spins with 3× spacing and
which form an aFM sequence as well as the primitive spin sequence with 1× spacing. In
fact, we may consider that the double arrows represent the spins of the Mn atoms in layers
without N (with N vacancies) - called Mn1 atoms, and that the single arrows represent the
spins of the Mn atoms in layers with N - called Mn2 atoms.

The SP-STM image produced using a Mn-coated W tip, at room temperature, is shown
in Fig. 3(a). There, two 90° rotated domains intersect along a domain boundary, which is
both a crystallographic as well as a magnetic domain boundary. Seen in either domain D1
or domain D2 is the row structure with 3× period in comparison to the primitive atomic
spacing. Clearly distinguishable is that adjacent rows have different brightness, and that
the brightness alternates from row to row. This brightness alternation is clearly seen in the
height profile shown in Fig. 3(b), which shows a modulation having period of 2 rows. Line
profiles from both domains D1 and D2 show the modulation, and a simple spin model of
the boundary region is depicted in Fig. 3(c). Clearly, the height modulation of the rows
corresponds to the aFM double arrow sequence previously given and the observation of a
modulation means that the SP-STM data contains two components - one magnetic and one
non-magnetic.

Seeing also that the magnitude of the height modulation shown in Fig. 3(b) is different
on the two sides of the boundary, in the inset of the model of Fig. 3(c), a probable vector
relationship is given for the tip spin and spins from either side of the domain boundary.
Yang *et al.* noted the cosine relationship for the amplitude modulation and derived the
tip-sample spin angle in their experiment to be ∼ 27°.

Yang *et al.* went on to show a method to separate the two components out from the
height profile. This method was explained mathematically in the paper and involved es-
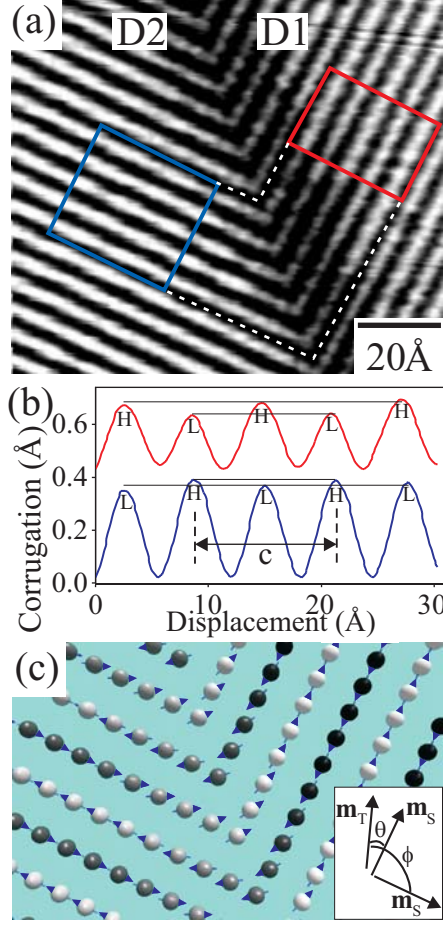sentially subtracting the π-shifted line profile from the non-shifted line profile to obtain the

FIG. 3: (a) SP-STM image acquired using a Mn-coated W tip at V_s = -0.6 V and I_t = 0.8 nA. (b) Two area-averaged line profiles (red and blue) corresponding to the regions inside the red and blue rectangles in (a). (c) Simulated SP-STM map: contrast: white↔black ⇒ θ: 0↔π. The inset shows the moments of tip ($\mathbf{m}_T$) and the sample ($\mathbf{m}_S$) for the two different domains and the angles between them. Each ball represents a magnetic atom (Reprinted with permission from H.Q. Yang, A.R. Smith, M. Prikhodko, and W.R.L. Lambrecht, Physical Review Letters **89**, 226101 (2002). Copyright (2002) by the American Physical Society).

magnetic part and adding these two to obtain the non-magnetic part. Doing so revealed a sinusoid-like non-magnetic component but a non-sinusoid-like (in fact, trapezoid-like) magnetic component at the bias voltage of V_S = -0.6 V. Consistent results were also obtained with an Fe-coated W tip.

Yang *et al* also went on to model the two components separately using LDOS values obtained from bulk first principles inserted into an atom-superposition model. Nice agreement

between theory and experiment was shown. Simulations based on the full Tersoff-Hamman model with surface LDOS calculated from first principles (by A. Dick and J. Neugebauer) were presented in a later paper by Smith *et al.*[15] That paper highlighted the shortcomings of the atom superposition method (i.e. comparisons of STM data to atom superposition simulations can be fortuitous - for reasons, see Ref.[15]) and underscored the importance of directional orbital lobes in SP-STM imaging and simulations.

III.E.3 Bias-Dependence of Spin Resolution of Mn_3N_2 (010)

Bias-dependence in atomic resolution images of surfaces is closely related to the spectroscopic information, and by studying the bias-dependence, additional information about the surface is often obtained. In the case of Mn_3N_2 (010), such data was recently reported (2004) by Yang *et al.* for the case of non-magnetic probe tips. What was clear from the bias-dependent CC height profiles was that the overall magnitude of the height profile was maximized near $V_S = +0.2$ V and that it gets smaller with increasing positive or negative voltage. This behavior was shown to be in good agreement with the amplitude values calculated based on atom superposition simulations using LDOS values calculated from bulk first-principles.

In the case of atomic-resolved magnetic STM images of the same surface, Smith *et al.* have investigated the magnetic amplitude dependence on the bias voltage, as recently reported (2005).[37] Shown in Fig. 4(a) is the sequence of spin-polarized STM images, acquired from the same exact surface location, of Mn_3N_2 (010) between $V_S = $ -0.6 V and $V_S = +0.6$V, in 0.2 V increments (not incl. 0). These images were acquired using an Fe-coated W tip. What is prominently seen in these images is the row structure, in which the observed atomic rows are centered at the Mn1 atoms.

Below each image in Fig. 4(a) is displayed the total CC height profile. Clearly, the data contains spin-resolved information, according to the evident modulation of the height profiles. Upward pointing red arrows, located at positively enhanced peaks, correspond to spin-↑; in-between, negatively enhanced peaks correspond to spin-↓.

To understand the experimental data more clearly, in Fig. 4(b) is a diagram showing a schematic spin-polarized STM line profile together with the atomic model of the Mn_3N_2 (010) surface, including magnetic moment vectors and labels of Mn1, Mn2, and N atoms.
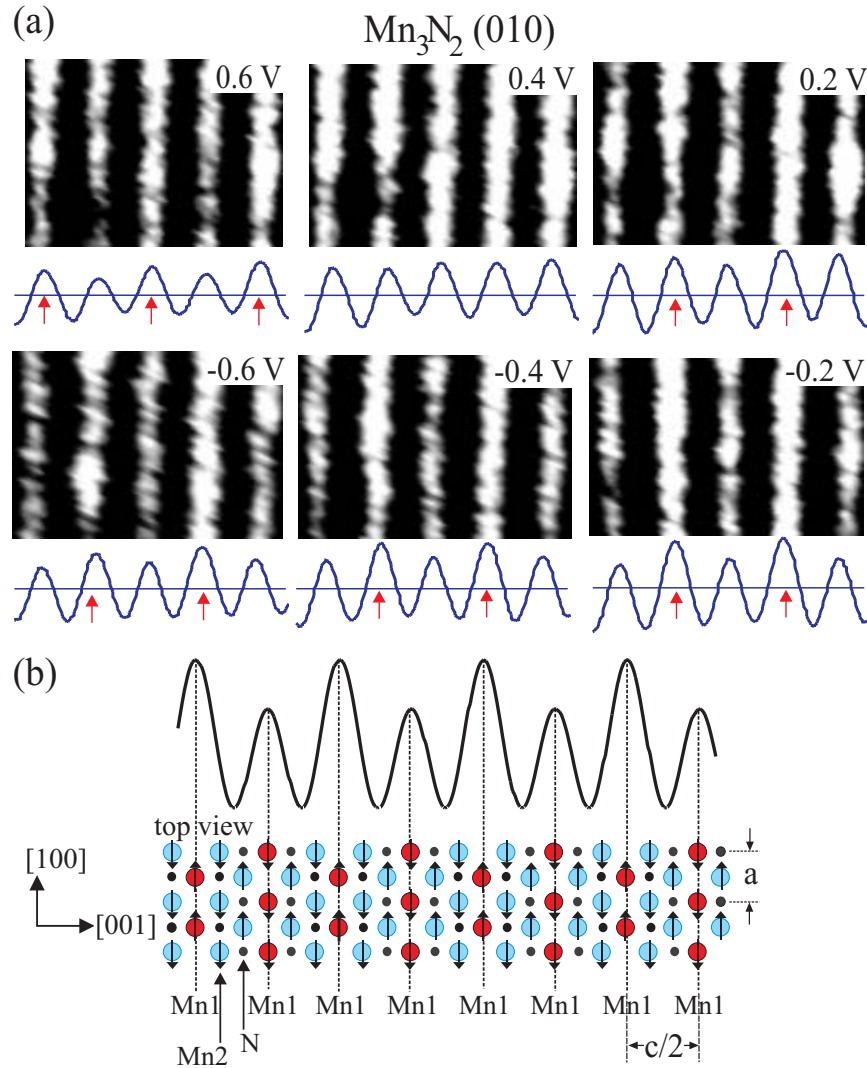
FIG. 4: (a) A series of SP-STM images of Mn3N2 (010) acquired using a Fe-coated W tip taken at the exact same surface location. The sample bias is indicated in each part, and tunnel current It = 0.3 nA. Height profiles below each image are averages over the vertical direction of the corresponding image; (b) diagram of spin-polarized STM line profile with atomic model of the Mn_3N_2 (010) surface, including magnetic moment vectors (Parts reprinted with permission of Wiley-Liss, Inc., a subsidiary of John Wiley and Sons, Inc., from A.R. Smith, R. Yang, H. Yang, A. Dick, J. Neugebauer, and W.R.L. Lambrecht, Recent Advances in Atomic-Scale Spin-Polarized Scanning Tunneling Microscopy, Microscopy Research and Technique **66**, 72 (2005). Copyright 2005 WILEY-LISS, INC.).
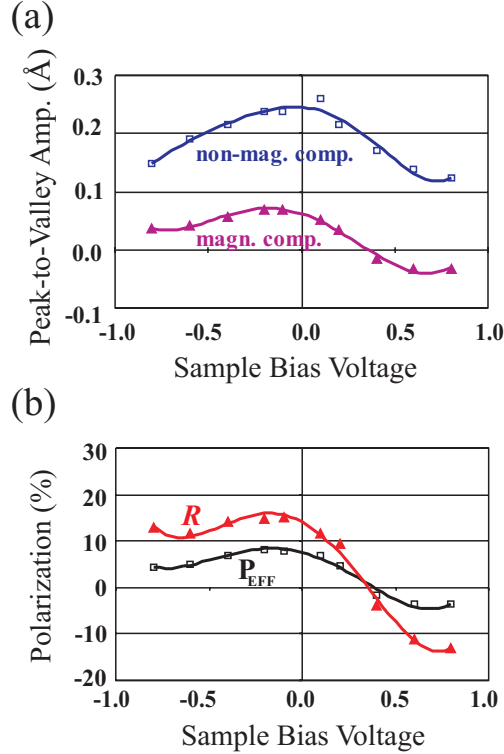
(a)

(b)

FIG. 5: Peak-to-valley amplitudes of magnetic (purple) and non-magnetic (blue) components of the height profile as a function of sample bias. (b) The deduced junction polarization P_{EFF} from STM data (black) and the ratio R of one-half the magnetic peak-to-valley amplitude to non-magnetic peak-to-valley amplitude vs. sample bias from STM data (red) (reprinted with permission of Wiley-Liss, Inc., a subsidiary of John Wiley and Sons, Inc., from A.R. Smith, R. Yang, H. Yang, A. Dick, J. Neugebauer, and W.R.L. Lambrecht, Recent Advances in Atomic-Scale Spin-Polarized Scanning Tunneling Microscopy, Microscopy Research and Technique **66**, 72 (2005). Copyright 2005 WILEY-LISS, INC.).

From this diagram, it is seen that the rows of the STM images are centered on the Mn1 atoms and that the height modulation of the rows corresponds to the alternation in magnetic vector direction of the Mn1 atoms.

Of particular interest in Fig. 4(a) is the observation of a magnetic contrast inversion point at $V_S \simeq +0.4$ V. At bias voltages less than +0.4 V, there are 2 high peaks and 3 low peaks in the series, whereas at bias voltage greater than +0.4 V (i.e. 0.6 V), there are 3 high peaks and 2 low peaks. This information is summarized in Fig. 5(a), which shows the experimental non-magnetic and magnetic amplitudes over an even larger number

of points. These values were obtained after separation of the magnetic and non-magnetic information contained within the data of Fig. 4(a). In Fig. 5(b) are shown two additional derived quantities: R = one-half the magnetic to non-magnetic amplitude ratio, and P_{eff}, the effective junction polarization, which was defined by Wiesendanger *et al.*[2]

The non-magnetic bias-dependent amplitude shows very good agreement with our previously published data using non-magnetic STM tips.[35] But here we want to focus on the magnetic amplitude. The important issue is whether this bias-dependence is a function of the sample electronic structure or that of the tip. As it is widely accepted, ever since the original work of Tersoff and Hamann,[38] that what the STM images in normal STM is the LDOS of the sample (not the tip) near the Fermi level, it is important to assess if this is also the case in magnetic STM. This can only be determined by performing careful first principles surface calculations and then inserting the results into a spin-polarized form of the Tersoff-Hamann formula. A new paper combining experiment and theory, addressing this exact issue, is being finalized in parallel with this review.[39]

III.F. Antiferromagnetic Fe Monolayer on W(001)

The interest in the magnetic properties of iron has existed surely since Man's earliest encounter with this material. Mainly, iron has proven to be one of the best ferromagnets ever known, in its bcc bulk structure. However, there has been much study to try to stabilize Fe in other magnetic states via different crystal structures or using novel strategies. One strategy is take advantage of low-dimensionality, such as a single ML of Fe (2-D) on a particular substrate. One such system - namely a ML of Fe on W(001) - was examined in the early 1990's, and clear experimental evidence was obtained - using spin-resolved photoemission[40] and Kerr effect measurements[41] - showing a lack of remanence and arguing against a FM ground state. Density-functional theory lent support to the possible existence of a lowest-energy aFM Fe ML state.[42]

In very recent work (2005), Kubetzka *et al.* demonstrated convincingly that a single ML of Fe on W(001) has indeed an aFM ground state, using atomic-scale SP-STM.[43] In this paper, they place their work well into the experimental and theoretical context but utilize the unique atomic-scale magnetic resolution capability of SP-STM to prove that the magnetic ground state is aFM c(2×2). The also show that the magnetization is *out-of-plane.*
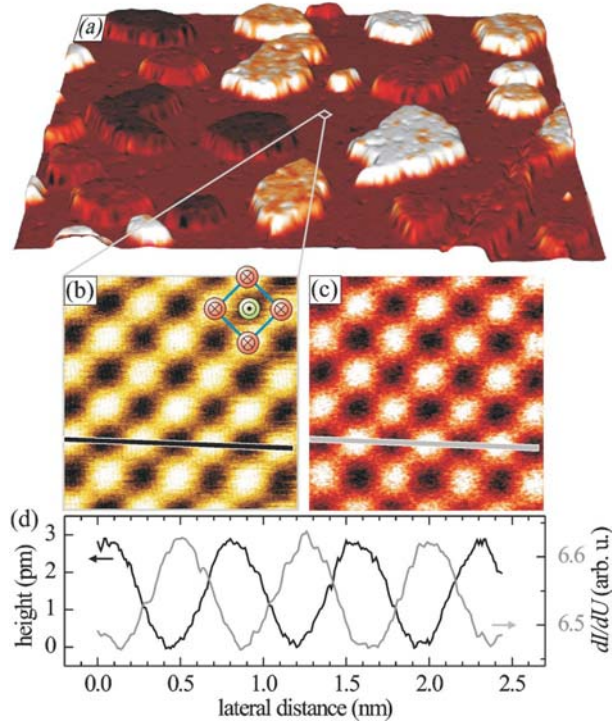
FIG. 6: (a) 3D composite of topography (height) and dI/dU signal (color) of a 100×100 nm^2 surface area of 1.3 ML Fe/W(001) ($I = 2$ nA, $U = 500$ mV). In zero field a four stage magnetic contrast is observed on the second layer islands. In an external field of $B = +2.5$ T the ML shows a $c(2\times2)$ superstructure in (b) the constant current image as well as in (c) the corresponding dI/dU map (2.5×2.5 nm^2, $I = 3$ nA, $U = -100$ mV). (d) Line sections along the [100] direction (Reprinted with permission from A. Kubetzka, P. Ferriani, M. Bode, S. Heinze, G. Bihlmayer, K. von Bergmann, O. Pietzsch, S. Blügel, and R. Wiesendanger, Physical Review Letters **94**, 087204 (2005). Copyright (2005) by the American Physical Society).

Shown in Fig. 6(a) is the large-scale image of the surface containing 1.3 ML Fe on W(001). Islands of the second layer are seen clearly within the area; their different color can be interpreted in terms of the FM vector orientation of these second layer islands. For a more general study of the morphological and magnetic structure of the Fe/W(001) system in the pseudomorphic regime, including islands up to the 4th ML, see the recent paper by Von Bergmann *et al.*[44] The focus of the atomic-scale SP-STM study is on the areas in between the second ML islands, which are the areas having just 1 pseudomorphic ML of Fe on W(001). Zoom-in images of a tiny area of the 1 ML Fe region are shown in Fig. 6(b)

and 6(c). Fig. 6(b) shows just the normal constant current STM image of the region, while Fig. 6(c) is the dI/dV spectroscopic image of the same region.

Clearly, both CC and dI/dV images show an atomic-scale checkerboard pattern, whose interpretation is well explained by Kubetzka et $al.$ As discussed previously, for the case of a Mn ML on W(110) published by Heinze et $al.$,[7] the first remarkable point is that in these images also, only magnetic contrast is observed; the normal atomic resolution image observed using a non-magnetic W tip would show twice as many bright spots. It turns out that the bright spots of Fig. 6(b), however, correspond only to the atoms of spin down, whereas the dark "holes" correspond to the atoms of spin "up" [see Fig. 6(b), model overlay]. As also clearly seen in Fig. 6(b) and 6(c), the CC and dI/dV images are 180° out of phase, as shown also in the line profile of Fig. 6(d).

To achieve this remarkable result, Kubetzka et $al.$ used an Fe-coated W tip which normally shows $in\text{-}plane$ magnetic contrast, in absence of an applied magnetic field. However, the images shown in Fig. 6 were not obtained in zero field but instead were obtained using the unique capability of their STM which allows application of large perpendicular magnetic fields of magnitude 2.5 T. They explain that such a field is sufficient to rotate the magnetization of the Fe-coated tip into the $out\text{-}of\text{-}plane$ direction. After doing this, the aFM contrast of the Fe ML is obtained. Then, knowing that in SP-STM, magnetic contrast is only seen for the case where sample and tip have a common vector component, it can be concluded that the sample magnetization is also $out\text{-}of\text{-}plane$. It is also understood here that the applied magnetic field, although rotating the FM tip magnetization vector, should leave the aFM layer magnetization unaffected.

In their paper, Kubetzka et $al.$ also present side-by-side images of a small surface region obtained in opposite magnetic fields of +2.5 T and -2.5 T. Such fields will polarize the FM tip coating oppositely, and both images show clear magnetic contrast, but 180° out of phase. Then by subtracting the two images, the purely magnetic image is obtained showing the clear c(2×2) aFM contrast, and by adding the two images, the purely non-magnetic image is obtained. Mathematically, this approach is equivalent to the difference/sum method used by Yang et $al.$ to separate out the magnetic and non-magnetic components from their SP-STM line profiles of Mn_3N_2 (010), as previously discussed. In Kubetzka et $al.$'s case, however, while the magnetic image shows clearly the aFM structure, the non-magnetic image does not show any underlying atomic features.

A nice outlook of the paper by Kubetzka *et al.* is the possibility to tune the substrate/overlayer interaction by varying the substrate lattice constant, for example through the use of alloys, with the possibility of obtaining a variety of new magnetic overlayer structures.

III.G. Antiferromagnetic NiO(001) Surface: Spin-Polarized *AFM*

Although SP-STM is limited to conducting samples, other investigators have recently been attempting to make use of the magnetic exchange force interaction as another means to detect spin direction at a sample surface. Atomic force microscopy (AFM) is well known as a method for imaging insulating as well as conducting samples. The use of non-contact AFM (NC-AFM) to study surfaces has proven to be successful for obtaining resolution down to atomic scale. If then a magnetic exchange interaction would exist between a magnetic probe tip and a magnetic surface, then a component of the total force interaction could be attributed to be of magnetic origin; and therefore, the NC-AFM image could potentially contain spin-dependent information.

A key question in recent years has concerned with what is the size of the magnetic exchange force which could be expected, and whether then it would be large enough to be detected. A number of theoretical calculations were published on this topic.[45–48] The conclusion of these works suggests that the exchange interaction between a FM tip and a FM sample would indeed be sufficiently large for detection using conventional NC-AFM available instrumentation.

The use of FM atomic force microscopy tips on FM sample surfaces is chiefly thought of as the method of magnetic force microscopy (MFM). The technique of MFM, however, has lateral spatial resolution limited to $\sim$ several 10's of nm, due to the fact that the relevant interaction is the long-range dipole interaction involving the stray field of the sample and tip. The long-range interaction has nothing to do with the exchange force as a means of spin measurement. However, to overcome the dominating effect of the long-range dipole interaction, and to obtain sensitivity to the much weaker short-range exchange interaction, an ideal approach is to utilize either an aFM tip, an aFM sample, or both.

In two recent (2004) papers, Hosoi, Sueoka, and co-workers have shown promising results using just this kind of approach.[49, 50] In their reported experiments, they have applied

ultra-high vacuum NC-AFM operating at room temperature, with 3 different types of probe tips: 1) Fe-coated Si tips; 2) Ni-coated Si tips; and 3) non-magnetic Si tips.

For their sample, they selected the well-known room-temperature aFM insulator NiO, and as the surface of study, NiO(001). The crystallographic model of NiO with spin alignment, as shown by the authors, is reproduced in Fig. 7(a). A key point is that along the [110] direction, spins are antiferromagnetically aligned, while along [1$\bar{1}$0] direction, spins are ferromagnetically aligned; this point is utilized in the analysis of Hosoi *et al.*

The sample and tip were each outgased under vacuum, using a mild heating step. The Si cantelever tips were coated by Fe (or Ni) to a coating thickness of 30 nm. The NiO(001) surface was prepared by cleaving the NiO bar in UHV.

NC-AFM images using the 3 different types of tips were obtained, each showing atomic resolution. In their papers, the authors present the image obtained using the Fe-coated Si tip. This image, reproduced in Fig. 7(b), shows a square array of atomic protrusions, whose vertical corrugations are ~ 0.3 Å; no obvious height differences can be seen in the image between the different protrusions. The authors give arguments to decide whether the protrusions observed correspond to the Ni or to the O atoms. A number of prior studies would suggest that it is the O atom which is the protrusion in images acquired using metallic probe tips.[51–54]

It is therefore concluded in the work of Hosoi, Sueoka, and co-workers that the NC-AFM image of NiO(001) obtained using the metallic-coated (Fe or Ni) probe tips show protrusions which correspond to the O atoms. They go on then to analyze in detail the line profile corrugations, looking for indication of spin contrast. While none appears in the image upon visual inspection, a method is presented to enhance the signal to noise ratio by superimposing groups of line scan pieces representing identical magnetic structure. This method is shown schematically by Hosoi *et al.*, as reproduced in Fig. 7(c). The results of the data processing for the data shown in Fig. 7(b) are reproduced in Fig. 7(d), where a slight difference in corrugation maxima between adjacent atomic sites along [110] can be detected.

To lend statistical significance to the relatively small effects, Hosoi, Sueoka, and co-workers define a quantity called topographical asymmetry $A = (A_u - A_d)/(A_u + A_d)$, with A_u and A_d being the maxima of the superimposed corrugations at the adjacent u and d atom sites, respectively. This quantity is computed for different azimuthal directions of the
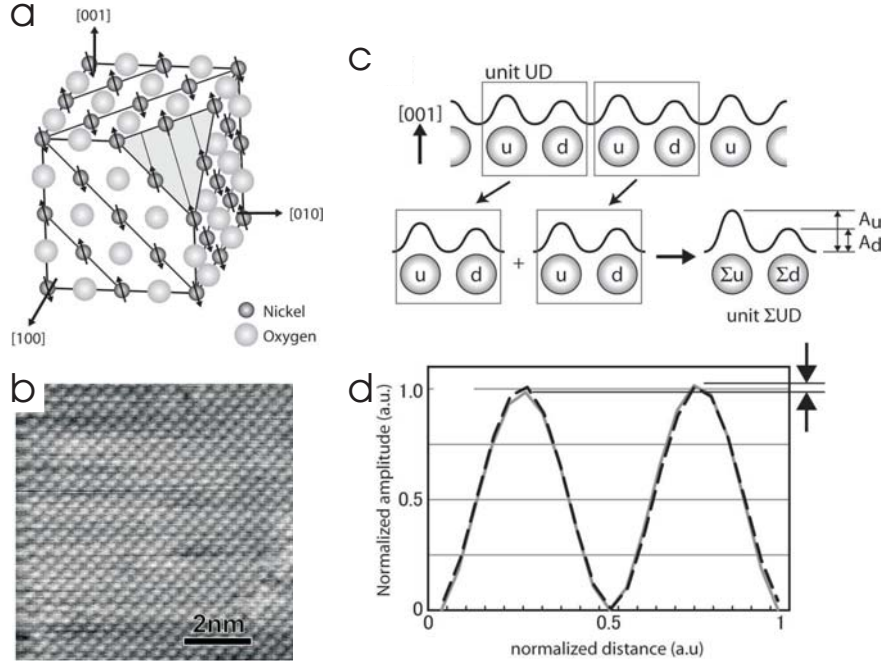
FIG. 7: (a) the crystallographic structure of NiO single crystal with spin alignment. The spins at Ni sites on {111} planes are ferromagnetically aligned, and the direction of spin in the adjacent planes is antiparallel; (b) atomically resolved image obtained with an Fe-coated tip (8.1 nm × 8.1 nm; (c) conceptual scheme of atomic corrugation analysis. The cross-section is divided into the unit cell (UD) composed of adjacent atoms u and d. Their corrugation amplitudes are added and the maximum values at each atom site are compared by means of topographical asymmetry; (d) the added corrugation amplitude taken from (b) in the [110] (full gray curve) and the [$1\bar{1}0$] (dashed black curve) direction (reprinted with permission of IOP Publishing Ltd, from H. Hosoi, K. Sueoka, and K. Mukasa, Investigations on the topographical asymmetry of non-contact atomic force microscopy images of NiO(001) surface observed with a ferromagnetic tip, Nanotechnology **15**, 505 (2004). Copyright 2004 IOP Publishing Ltd).

surface.

As discussed by Hosoi and co-authors, by comparing A along [110] vs. A along [$1\bar{1}0$], a difference can be seen, with A almost 1.5% for [110] vs. $\sim 0.4\%$ for [$1\bar{1}0$]. The authors then proceed to tabulate results from the various magnetic-coated and non-magnetic-coated tips in the same way, and based on those numbers, they argue that the magnetic-coated tips show statistically significant magnetic effects in comparison to the non-magnetic Si tips.

However, they do note some inconsistencies among the different tips, for which they present some possible explanations.

Assuming that these very small measured asymmetries are reliable, then it is important to understand their origin. One of the key points raised in the works by Hosoi, Sueoka, and co-workers is that although the protrusions correspond to O atoms, the magnetic moments in NiO are carried by the Ni atoms; how then, can one understand the observed corrugation asymmetries? This question is addressed in a recent first-principles theoretical study by Momida and Oguchi.[55] They study exactly the NiO system realized by Hosoi and co-workers. One of the key points in their work is that the surface O takes on a moment due to surface symmetry breaking, although it is small ($\sim 0.07\ \mu_B$). This is due to hybridization between the surface O atom p states and the second-layer Ni atom d states. Moreover, the first-layer O atom moment is parallel to the second-layer Ni atom moment, rendering the same aFM surface symmetry for O atom sublattice as for Ni atom sublattice.

While the approach of NC-AFM to image magnetic structure by means of the exchange force interaction will require more study to fully understand, the work of Hosoi *et al.* represents the ultimate in what has been achieved to date in atomic-scale SP-AFM imaging. Although this method offers applicability to insulating materials such as NiO, the sensitivity of the method appears to be a significant potential limitation.

IV. ATOMIC-RESOLVED SPIN-STRUCTURE IN FERROMAGNETS

Although antiferromagnets are ideal subjects for observing atomic-scale spin variations, or alternations, the power of the SP-STM is its ability to detect either changes in the local spin direction, or changes in the local spin-polarization density. In the case of a ferromagnet, unless in the proximity of a domain wall, one would not expect to observe changes in spin direction. Thus the atoms of a given surface would appear identical, even given the use of a magnetic tip and even in the presence of applied magnetic fields.

A recent work (2004) by Berdunov *et al.* presents a unique experiment using SP-STM to examine the spin-structure of FM magnetitite (Fe_3O_4).[56] Magnetite is currently of great interest for its possible use as a spin-injection electrode in devices such as magnetic tunnel junctions. Berdunov *et al.* present interesting results on the (111) face of Fe_3O_4. Their sample surface was produced using an oxidizing procedure which results in a stable oxygen

termination. The surface structure then consists of a lattice of O atoms (first layer) on top of an Fe layer (second layer). With only few surface O vacancies, the surface forms a hexagonal superstructure having periodicity of ~ 42 Å, which is explained as being due to an electron-lattice instability.[57]

Berdunov *et al.* study this surface using magnetic STM tips in a UHV STM system at room temperature. For the magnetic tip, they chose to use a MnNi alloy in the form of rods which are electrochemically etched to produce sharp tips. MnNi (1:1 stoichiometry) is an aFM compound with a high Néel temperature (~ 800°C) having the tetragonal CuAu-I type structure, one of a family of such materials.[58–61] One advantage of an aFM tip is to avoid possible stray field effects on the sample under study.

To explore the success of the MnNi tip preparation procedure, an Auger spectroscopy study was performed on a similarly prepared MnNi disk.[62] In fact, this study indicated preferential sputtering during the final *in-vacuum* preparation (ion etching) step, leaving a Ni-rich phase.[58] If this also occurs for the case of the tip etching, then a thin FM layer might have formed at the tip apex. But in any case, the tip so produced would presumably be spin-polarized with small, or negligible, stray field.

Under zero applied magnetic field, Berdunov *et al.* obtained STM images like that reproduced in Fig. 8(a), which shows extended areas of bright and dark, corresponding to the large-scale superstructure. The little protrusions are interpreted as the O atom sites, whose spacing depends on the exact location within the superstructure, but is ~ 3 Å. A number of small O vacancies are observed, which appear as holes [circled in the image of Fig. 8(a)]. No sign of any spin-polarized effect is seen in this image.

Under a magnetic field of 60 mT applied parallel to the surface of the sample, a different image was obtained, as reproduced in Fig. 8(b). This image shows the same superstructure features as with no magnetic field. However, it shows that in the vicinity of the O vacancy sites, there appear three bright spots, which are not seen in the absence of applied magnetic field. The height of the bright spots in relation to the surrounding O sites is measured to be ~ 0.3 Å. The separation of the bright spots (6 Å), and their positions, are stated to correspond to the positions of Fe ions in the layer underneath the topmost O layer. According to the authors, the bright spots have a magnetic origin.

Berdunov *et al.* apply the basic tunneling equation (which assumes a constant sample LDOS) at the position of the bright spot and also at the position of an O site, in order to
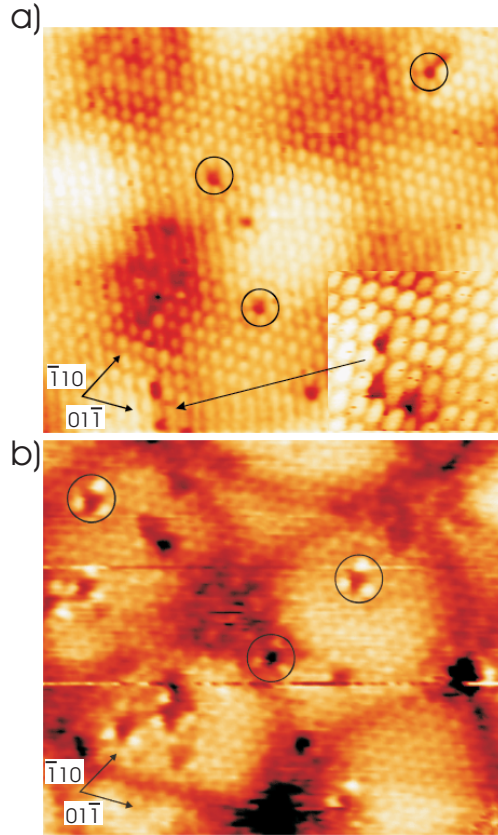
FIG. 8: STM images (10.5×8.5 nm^2 and 7×8 nm^2) of the superstructure without (a) and with magnetic field (b). Circles mark the oxygen vacancies in the topmost surface layer. (b) Three bright spots appear around vacancy that correspond to Fe sites with 6 Å interatomic distance. ($V_{bias} = -1.0$ V, $I_t = 0.1$ nA, MnNi tip). Inset in (a) shows a high resolution image of the defects (Reprinted with permission from N. Berdunov, S. Murphy, G. Mariotto, and I.V. Shvets, Physical Review Letters **93(5)**, 057201 (2004). Copyright (2004) by the American Physical Society).

determine the tunneling conductance at those points. From these numbers, the conductance variation is determined to be $\sim 250\%$, showing that the bright spots represent a sizeable spin-polarized effect.

To understand more clearly what is the origin of the conductance increase at the Fe site under the applied *in-plane* magnetic field, other experiments and some calculations were also reported. For example, Berdunov *et al.* reported in another paper that vibrating sample magnetometry measurements indicated that 60 mT is sufficient to fully saturate the magnetization of the sample.[63] In their related paper, Murphy *et al.* state that they

expect that the sample has *out-of-plane* ([111]-oriented) magnetization in zero-field, but that the applied 60 mT field rotates the magnetization to *in-plane*.[58] However, this by itself still does not explain the enhancement above the Fe sites near the O vacancies, since their magnetization is assumed to be parallel to that of the rest of the sample.

To find a plausible explanation of the observed effect, it is necessary to consider the effect of the O vacancy on the LDOS of the sample, in particular on the spin-polarized LDOS. According to a previous paper by Tsymbal *et al.*, the surface O atom orbitals of the ideal O-terminated surface (without vacancies) become conductive through hybridization of the O *p*-states with the transition metal (Fe) *d*-states.[64] According to the plots of spin-polarized DOS shown by Berdunov *et al.*, obtained from their first-principles calculations, the surface O sites then become spin-polarized just as with the underlying Fe atom sites. This is particularly true over the range from the Fermi level to 1 eV below the Fermi level, which corresponds to the energy window (V_{bias} = -1 V) of their experimental SP-STM image. The spin-polarization over this window is, however, much larger for the second-layer Fe states than for the surface O states.

To understand the obtained magnetic effect as explained by Berdunov *et al.*, it is necessary to consider that in the vicinity of the O vacancy, the spin-polarization of the Fe states is altered, presumably due to changes in the hybridization of *p* and *d* orbitals. Plausibly, this could result in a local increase in the spin-polarization at the Fe atom sites directly adjacent to the O vacancy. In their paper, the authors present plots of spin-up electron density above the O-terminated surface, both with and without an O vacancy. Clearly, the spin-up electron density at specific sites is altered by the presence of the vacancy.

From the experimental point of view, however, this still does not explain why the bright features were not seen in the image under zero applied magnetic field, using spin-polarized STM with the MnNi tip. A plausible explanation (not put forth by Berdunov *et al.*) could be that by applying the *in-plane* magnetic field, the magnetization of the sample was rotated into alignment with the magnetic vector of the tip. In this case, then, the spin-polarized tunneling current could be enhanced at the point with greatest spin-polarized LDOS, such as above the Fe atoms adjacent to the O vacancy. This would imply that the magnetization of the MnNi tip was parallel to the sample surface. In absence of applied field, magnetization vectors of sample and tip would be orthogonal, resulting in no spin-polarized contrast.

In any case, the results presented by Berdunov and co-workers in their recent series of

papers represents a very interesting observation of atomic-resolved spin-polarized imaging. The ability to detect local changes in the spin-polarization of ferromagnets, down to the atomic scale, opens new vistas for the technique of atomic-resolved SP-STM.

V. THEORETICAL BASIS FOR ATOMIC SCALE SPIN-RESOLVED STM

In tandem with the various atomic-scale SP-STM experiments which have been reported within the last five years, a variety of theoretical studies have also been published. Many of these studies have been performed in collaboration with the experimental efforts, though not all. In this section is discussed the current state of the art in theories of atomic-scale SP-STM, including comparative discussions across the range of published experimental results.

V.A. Fourier expansion in reciprocal lattice vectors: star functions and star coefficient theory

V.A.1 Magnetic signal dominant

The original paper of Heinze *et al.* on the topic of Mn ML/W(110) was a combination of theory and experiment.[7] Shortly thereafter (2001), Wortmann, Heinze, and colleagues published a second, theory-only paper in which they laid down basic theory of spin-polarized tunneling and then applied it to make SP-STM simulations of a Cr ML on Ag(111).[16] In that paper is introduced the extension of the Tersoff-Hamann equation to the spin-polarized case, and an expression is given for the tunneling current in terms of the non-magnetic and magnetic LDOS of sample and tip, similar to equation (2) given here.

The paper of Wortmann *et al.* reiterated the point made in Heinze *et al.*'s work that the magnetic signal in CC imaging mode of Mn ML/W(110) dominated completely the chemical atom (non-magnetic) signal. And in their STM simulations of Cr/Ag(111), a model spin-frustration system, the same effect is also predicted.

The theory for this behavior is explained well within the work of Heinze *et al.* and Wortmann *et al.* - namely in terms of the reciprocal lattice vectors $G_\parallel$ of the magnetic structure in comparison to those of the non-magnetic structure. As explained, an SP-STM image can be written as a 2D Fourier expansion in reciprocal lattice vectors, in which the

$G_\parallel$'s appear in the expansion coefficients as exponents of damped exponentials. Therefore, the larger the $G_\parallel$, the smaller the expansion coefficient. As the non-magnetic lattice will have the largest $G_\parallel$'s, it will be the most strongly damped.

Bode *et al.*, in a very thorough and explicatory paper (2002), defined the reciprocal lattice vector Fourier expansion in terms of "star functions" and "star coefficients."[65] The star coefficient theory applied to Mn ML/W(110) is also discussed at length in another paper by Heinze *et al.*[66] This theory strengthened the reciprocal lattice vector theory by considering that the electronic states of the surface, relevant to specific length scales, are contained within the star "coefficients." Hereafter, I refer to this theory as the star coefficient theory.

V.A.2 Magnetic signal a perturbation

The star coefficient theory, with which the recent (2005) work of Kubetzka *et al* on Fe/W(001) is in good agreement, preceded the work of Yang *et al.*'s 2002 paper, in which it was shown that both magnetic and non-magnetic contrast were obtained in, and could be separated from, a single atomic-scale SP-STM image of aFM Mn_3N_2 (010).[14]

In Fig. 9 is reproduced from Ref.[37] a comparitive diagram between the SP-STM results on Mn_3N_2 (010) of Yang *et al.* and the Mn ML/W(110) of Heinze *et al.* As can be seen, the spatial arrangement of Mn atoms is very similar for the two different systems. In either case, the surface Mn atoms form a centered rectangular lattice with their magnetic moments alternating in direction from row to row, with rows along [100] for Mn_3N_2 (010) and along [001] for Mn/W(110). Although the lattice constants and a:b ratios are slightly different, for comparison purposes in Fig. 9 the two lattice models have been normalized along the x-direction.

It is also important to note the existence of two chemically inequivalent Mn atom sites on Mn_3N_2 (010), Mn1 and Mn2. As discussed thoroughly in Ref.[37], the result is that the two inequivalent Mn sites completely changes the non-magnetic periodicity of the surface. Since the magnetic superstructure of Mn_3N_2 (010) has a period of 6 individual atomic rows, compared to the case of Mn/W(110) of 2 individual atomic rows, the associated reciprocal lattice vectors (magnetic and non-magnetic) are comparatively smaller; therefore, one may expect that it will be possible to observe both the magnetic and non-magnetic components.
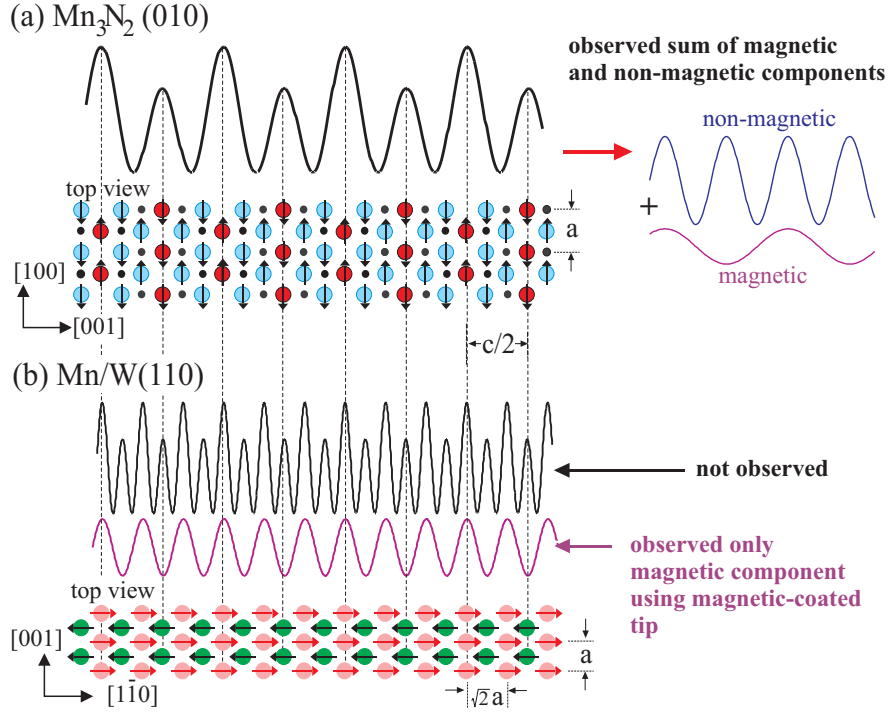
FIG. 9: Comparative diagram between SP-STM results on Mn_3N_2 (010) by Yang *et al.* and Mn ML/W(110) by Heinze *et al.* (a) schematic total line profile with top view surface model of Mn_3N_2 (010) and separated components; (b) schematic line profile obtained (only magnetic) with top view surface model of Mn ML/W(110); also shown is the fictitious total line profile including non-magnetic part which was not obtained. Surface models have been normalized to have the same x-direction atomic row spacing (reprinted with permission of Wiley-Liss, Inc., a subsidiary of John Wiley and Sons, Inc., from A.R. Smith, R. Yang, H. Yang, A. Dick, J. Neugebauer, and W.R.L. Lambrecht, Recent Advances in Atomic-Scale Spin-Polarized Scanning Tunneling Microscopy, Microscopy Research and Technique **66**, 72 (2005). Copyright 2005 WILEY-LISS, INC.).

It should be noted, however, that in Yang *et al.*'s work, the non-magnetic signal has *larger* amplitude than the magnetic signal at all measured bias voltages between -1.0 V and +1.0V; this behavior would therefore seem to not necessarily agree with the predictions of the star coefficient theory. However, it may not disagree, if the spin-polarized electronic states of the sample, and the electronic structure of the STM tip as well, are taken into account.

In fact, Bode *et al.* discuss the importance of first-principles calculations to identify the electronic states contained within the particular star coefficients, noting that if there are no states contained within the star coefficient of the smallest nonvanishing reciprocal lattice

vector, then the STM image will be dominated instead by the star function of the next larger reciprocal lattice vector.

The case of Fe_3O_4 (111) reported by Berdunov *et al.* may also be reconsidered in comparison with the star coefficient theory. As reproduced in Fig. 8(b), it is clear that in the applied-field case, the magnetic protrusion is a feature which is superimposed on the oxygen corrugation. Berdunov *et al.* state in their paper that the bright spots seen under applied field correspond with the positions of the underlying Fe atoms having spacing of 6 Å; whereas, the surface O atom spacing is only ~ 3 Å. We may therefore consider that the star wavefunction corresponding to the Fe atoms has the smallest reciprocal lattice vectors and should therefore be dominant in the image. And in fact, this appears to be the case, comparing with the O atom corrugation surrounding the bright spots. From this perspective, the Fe_3O_4 (111) case is consistent with star coefficient theory.

Finally, we may reconsider the case of NiO(001) imaged using SP-AFM with magnetic-coated tips, as reported by Hosoi and co-workers. Clearly, as reproduced in Fig. 7(d), the magnetic corrugation is truly a tiny modulation on top of the non-magnetic corrugation, despite the fact that the reciprocal lattice vectors corresponding to the magnetic unit cell are the smallest non-zero ones. We can therefore say with fair certainty that the star coefficient theory does not hold for atomic-scale SP-AFM; but this is not unreasonable, since the exchange force imaging mechanism is completely different and needs more study.

V.A.3. Atomic-scale magnetic imaging using dI/dV mode

Along with CC mode magnetic imaging at the atomic-scale, Wortmann *et al.*[16] discuss briefly the spectroscopic mode, considering that the derivative of the tunneling current equation has the form:

$$dI_t/dV \sim \frac{1}{2}[n^t n^s + m^t m^s cos\theta] \tag{3}$$

Eq. (3) is the basis for the highly successful application of the spectroscopic dI/dV mode utilized by Wiesendanger and co-workers to obtain the dramatic results on domains and domain walls of various transition metal surfaces.[2–10] It is so successful because the dI/dV mode allows to lock onto the magnetic signal where it is maximized at a specific voltage, and it is not overwhelmed by the non-magnetic (topographic) signal.

Despite this advantage, Wortmann *et al.* argued that the dI/dV method was inapplicable to reveal complex atomic-scale spin structures, partly due to the perceived resolution limitation in dI/dV imaging to about 1 nm; this turns out not to be a limit at all, as reproduced in Fig. 6(c) from the recent (2005) work of Kubetzka *et al.*, who show dI/dV resolution of single atoms (nearest neighbor spin-↑-spin-↑ atom spacing of 4.476 Å). Kubetzka *et al.* have certainly shown that dI/dV mode is applicable to atomic-scale SP-STM measurements.

V.B. Inclusion of tip electronic structure

Without a doubt, the spin-polarized electronic structure of the STM tip plays a crucial role in atomic-scale SP-STM. In this section are described theoretical calculations in which the electronic structure of the tip is included.

V.B.1 Case of Mn ML on W(110)

In a paper published subsequent to Heinze *et al.*'s 2000 work on the Mn ML on W(110), Hofer and Fisher revisit the magnetic STM imaging of that surface using first-principles theory, with the intent to determine the extent to which current theory is able to reproduce the parameters observed in the experiment.[67] In their paper, they describe their theoretical work in which they compute the STM currents and corrugations using Bardeen's integral.[68] Several interesting points were determined from their analysis.

First of all, Hofer and Fisher not only computed the ground state of the pseudomorphic Mn/W(110) system, they also compute the electronic properties of the tip, assuming particular models for the tip. The first key result which they find concerns the simulation using the clean W tip. Interestingly, they found a corrugation of only 0.02 Å, as compared with Heinze *et al.*'s experiment, which found a non-magnetic corrugation of 0.15 Å. Bode *et al.* explain this discrepancy as a well-known deficiency of the Tersoff-Hamann model in predicting atomic-resolved corrugations of close-packed metal surfaces and also relate it to the diminishingly small size of the associated 3rd star coefficient in comparison to the 2nd star coefficient.[65]

On the other hand, calculated STM images using an Fe-atom tip (Fe apex atom on a W film) resulted in the opposite effect - namely a magnetic image having the same qualitative

symmetry as found in Heinze *et al.*'s experiment but a corrugation of 0.73 Å, in comparison to the much smaller corrugation found in the experiment of 0.03-0.04 Å (Fe-coated W tip) or < 0.01 Å (Gd-coated W tip). Hofer and Fisher also present their result for a Mn-atom tip (Mn apex atom on a W film), finding a much reduced magnetic corrugation of 0.18 Å. While it may be supposed that a further corrugation reduction could occur due to misalignment of the tip and sample magnetic axes, Hofer and Fisher conclude that in the actual experiment of Heinze *et al.*, the tip had most likely become coated with Mn atoms from the surface.

In a subsequent (2003) paper, Hofer and Fisher show new calculations in which they consider specific tip models of even more direct relevance to the actual experiment - particularly considering Fe atom tips contaminated with various amounts of Mn.[69] They show explicitly, for different tip models, the corresponding theoretical STM images with associated predicted corrugations. An interesting finding is that a dramatic reduction in corrugation amplitude occurs (0.89 Å $\Rightarrow$ 0.04 Å) upon replacing a Mn-contaminated tip (modeled as an Fe(100) facet tipped with a single Mn apex atom) with a highly Mn-contaminated tip (modeled as an Fe(100) facet coated with a Mn layer and tipped with a Mn apex atom).

Lastly, we consider the tunneling current question. In Hofer and Fisher's calculations for Mn ML/W(110), the median tip-sample distance used was 4.5 Å, corresponding to a tunneling current of 0.1 nA (Fe-atom tip) or 0.2 nA (Mn-atom tip). These typical STM tunneling currents are to be compared with the actual value reported (40 nA) for the experiment of Heinze *et al.* Such a large tunneling current would, in Hofer and Fisher's simulation, put the tip-sample system so close as to be in mechanical instability.[70] Reasoning further, they conclude that no method of STM simulation, based on ground state density functional theory, can explain the high current quoted in the experiment. A possible explanation for this discrepancy is found in their more recent (2003) paper.[69]

V.B.2 Case of Fe ML/W(001)

It is interesting to hypothetically extend these results to the case of the aFM Fe ML/W(001) recently reported experimentally by Kubetzka *et al.*[43] For a Fe tip (modeled as an Fe(100) facet tipped with an Fe apex atom) applied to the Mn ML/W(110), Hofer and Fisher predict a theoretical corrugation of 0.68 Å. Thus it would suggest that Fe-coated W tips should normally be capable of high atomic-scale corrugations. However,

in the reported experiment on Fe ML/W(001), in which Fe-coated W tips were used, the measured CC corrugation was slightly less than 0.03 Å; and, since this data was acquired with applied magnetic field (+2.5 T) which forced the tip magnetization vector perpendicular to the surface, combined with the *out-of-plane* anisotropy of the Fe ML deduced in the experiment, the tip and sample magnetizations should have been collinear during the measurement. Based on that, it is reasonable to assume that 0.03 Å represents the maximum corrugation achievable in the experiment. And there could have been no possibility of Mn contamination in this experiment. It would be therefore interesting to know what corrugations would be predicted by theory for the Fe ML/W(001) for various types of tips.

Concerning the tunneling current in the case of Fe ML/W(001), Kubetzka *et al.* reported a value of just 3 nA for the image reproduced here in Fig. 6. However, in the other STM figure of their paper, they report a value of 30 nA. Possibly the same explanation for the large tunneling current in the Mn ML/W(110) case would apply to this case, since both experiments were performed in the same STM system.

V.B.3. Case of Mn_3N_2 (010)

The Mn_3N_2 (010) surface offers exciting possibilities for testing atomic-scale SP-STM both experimentally and theoretically. In a previous section, original data of Smith and co-workers has been displayed, which shows that the magnetic properties of this surface are both interesting and complex. The complexity arises upon considering that the size of the magnetic period is a full 6 primitive atomic rows. Contained within that magnetic period are two rows of Mn1 atoms and four rows of Mn2 atoms. Therefore, in theoretical calculations, one must take into account the electronic states from both the Mn1 and Mn2 atoms. The corresponding size of the magnetic unit cell renders these calculations highly non-trivial. The N atoms have much lower LDOS and so contribute little to the tunneling current.

Concerning the key parameters of the SP-STM experiment on Mn_3N_2 (010), it is noted that while the bias voltage ranged from -1.0 V to +1.0 V, the tunneling current used was quite typical, i.e. 0.3 nA (Fig. 4 data). The magnetic amplitude reached a maximum of ~ 0.07 Å at $V_S = -0.15$ V, but it decreases to zero at $V_S \simeq +0.4$ V; above 0.4 V, the magnetic corrugation becomes negative due to the polarization reversal. The non-magnetic amplitude for the same data set reached a maximum of ~ 0.26 Å at $V_S = +0.1$ V and gets smaller

in either direction. Note that the maximum magnetic contrast is larger than the magnetic contrast reported by either Heinze *et al.* or Kubetzka *et al.*

Dick and Neugebauer have recently (2004) reported first-principles density functional theory calculations for the Mn_3N_2 (010) surface.[15] The theory used in this work is based simply on the spin-generalized Tersoff-Hamann model. The local density of states is first calculated using plane waves; however, to overcome certain calculational problems encountered for tip-sample distances > 3 Å, the wavefunctions were projected from the plane wave basis onto a basis set of atomic orbitals. Various tip models are utilized in order to generate the simulated STM images.

To compare with the experimental data at one interesting bias point, the Tersoff-Hamann simulations were carried out at $V_S = -0.2$ V. In the simulation, the tip-surface distance was 5 Å with effective tip spin polarization of 90%. Using these parameters, and with a single atom tip, the Tersoff-Hamann simulation found a total SP-STM height profile showing very little magnetic modulation; decomposition of the profile into its magnetic and non-magnetic parts revealed the reason why. The magnetic profile was highly oscillatory, showing magnetic contrast at each of the six Mn atomic rows which are aFM (see Ref.[15]). The non-magnetic corrugation was 0.36 Å, while the magnetic corrugation was 0.17 Å. Comparing this result with the corresponding atom-superposition simulation illustrated a key point regarding spin-polarized Tersoff-Hamann, that it is not the sphere-integrated (around the surface atom nucleus) LDOS which is most relevant, but instead the highly directional orbital lobes probed by the STM tip.

In the Mn_3N_2 (010) case, the relevant surface orbital lobes were mainly of Mn sd character. Contour plots of the magnetic spin density (LDOS) for Mn_3N_2 (010), together with a schematic view of the atomic and magnetic structure of the top surface layer, are reproduced from Ref.[15] in Fig. 10. What is nicely seen in Fig. 10 is that, e.g. for the central Mn atom, its sphere-integrated magnetic LDOS is positive (spin-$\uparrow$); whereas, in the region at the surface probed by the STM tip, the spin density is clearly negative (spin-$\downarrow$).

V.B.4. Mn_3N_2 (010): A multi-atom tip apex model

Because of this orbital lobe directionality, the single magnetic atom tip in Tersoff-Hamann simulation resulted in an aFM period of only 2 atomic rows for Mn_3N_2 (010) at $V_S = -0.2$
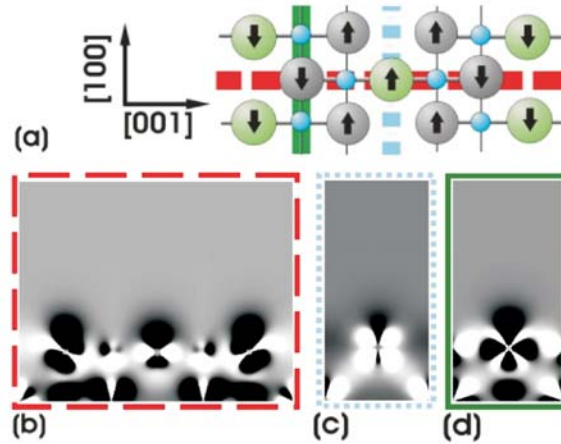
FIG. 10: a) Schematic view of the atomic and magnetic structure of the top surface layer. The arrows inside the atoms indicate the sign of the magnetic moment as determined by ILDOS at bias voltage V_s = -0.2 V, i.e. by integrating corresponding LDOS over a sphere around each atom and over energy. (b) , (c) and (d) show contour plots of the magnetic LDOS for the case of V_s = -0.2 V where bright and dark regions correspond to spin-up and spin-down densities correspondingly. The contour plots shown are the cross-sections through the surface layer along [001] axis (b) and the [100] axis (c, d). Horizontal and vertical bars of (a) show cross-section position of (b), (c), and (d) correspondingly (Reprinted from Surface Science **561**, A.R. Smith, R. Yang, H. Yang, W.R.L. Lambrecht, A. Dick, and J. Neugebauer, Aspects of spin-polarized scanning tunneling microscopy at the atomic scale: experiment, theory, and simulation, 154-170, Copyright (2004), with permission from Elsevier.).

V, not seen in the experiment. However, to reproduce the experiment, Dick and Neugebauer have not applied the star coefficient theory, but rather have continued with Tersoff-Hamann directly and instead applied a multi-atom tip apex. In particular, they applied a 4-atom magnetic tip consisting of four non-interacting s-like atoms locating at the corners of a square and lying in a plane parallel to the surface.

Corrugation profiles based on this 4-atom tip apex model are shown in Ref.[15] Essentially, the 4-atom tip results in overall very good agreement with the experiment. The total corrugation profile appears as a modulated sinusoid as in the experiment, and the separated components have both the correct shape and periodicity of the experimental ones. Numerically, the non-magnetic component has a corrugation of 0.19 Å, a little smaller than in the

experiment (0.24 Å), whereas the magnetic component has a corrugation of 0.05 Å, also a little smaller than in the experiment (0.07 Å). Note, however, that the predicted magnetic corrugation would be ∼ a factor of 2 smaller if an effective tip polarization of 44% was used, similar to that assumed for Fe-coated W tips by Bode *et al.*[3] Dick and Neugebauer also explored the effect of varying the tip apex atom-to-atom distance as well as the tip-surface distance, and those effects are also described in Ref.[15]

V.B.5. Case of Fe$_3$O$_4$ (111)

Lastly, it is interesting to briefly reconsider the case of Fe$_3$O$_4$ (111) reported by Berdunov *et al.*[56] quantitatively. The tunneling conditions certainly are typical for STM (V_{bias} = −1.0 V, I_t = 0.1 nA). The corrugation difference between the magnetic feature (bright spot) and the surrounding atomic structure was reported to be 0.3 Å. Comparing with the measurements already discussed for aFM surfaces, this experimental magnetic corrugation is actually quite large [more than 4× as large as the maximum magnetic corrugation measured for Mn$_3$N$_2$ (010), 0.07 Å], especially considering that the signal is attributed to the enhanced magnetization of a second-layer Fe atom; of course, a strong hybridization between surface O states and second-layer Fe states was found. It would be interesting, however, to have a calculation which tries to take into account the tip structure.

VII. SUMMARY

This paper has attempted to provide the reader with a reasonably thorough discussion of recent advances in spin-resolved probe microscopy, mainly tunneling microscopy, including a number of the chief experimental works as well as important theoretical papers. Overall, it is found that major progress has been made in this field within 6 years (c. 2000 - 2005). Experiments have succeeded to resolve exceedingly fine details of magnetic structure of various surfaces and to determine ground state magnetic structures in systems where non-SPM-based experimental methods could only obtain evidence indirectly. Truly, the atomic-resolved SP-STM represents the ultimate in 2D spin-resolving techniques.

Tersoff-Hamann theory has been successfully extended to the atomic-scale spin-polarized case, and in combination with first-principles density functional theory, has been applied

with great success to model the experimental results. A variation of this - referred to as star coefficient theory - has been discussed and its validity examined. In general, it appears to describe well many of the experimental findings. The electronic structure of the STM tip remains an apparent key ingredient in the STM calculations. Future theoretical work will not likely avoid to take it into account.

In the future, we may expect that experimentalists will continue to surprise with further dramatic displays of spin-resolved surface structures. Going beyond this, the day may not be far off when experimentalists succeed to engineer specific magnetic structures at the atomic scale and, using the power of SP-STM, directly verify their magnetic structure step by step.

ACKNOWLEDGEMENTS

[1] G. Binnig, H. Rohrer, C. Gerber, and E. Weibel, Appl. Phys. Lett. **40(2)**, 178 (1982).

[2] R. Wiesendanger, H.-J. Guntherodt, G. Guntherodt, R. J. Gambino, and R. Ruf, Phys. Rev. Lett. **65**, 247 (1990).

[3] M. Bode, M. Getzlaff, and R. Wiesendanger, Phys. Rev. Lett. **81**, 4256 (1998).

[4] R. Wiesendanger, M. Bode, and M. Getzlaff, Appl. Phys. Lett. **75**, 124 (1999).

[5] O. Pietzsch, A. Kubetzka, M. Bode, and R. Wiesendanger, Science **292**, 2053 (2001).

[6] M. Bode, S. Heinze, A. Kubetzka, O. Pietzsch, X. Nie, G. Bihlmayer, S. Blügel, and R. Wiesendanger, Phys. Rev. Lett. **89**, 237205 (2002).

[7] S. Heinze, M. Bode, A. Kubetzka, O. Pietzsch, X. Nie, S. Blügel, and R. Wiesendanger, Science **288**, 1805 (2000).

[8] M. Kleiber, M. Bode, R. Ravlic, and R. Wiesendanger, Phys. Rev. Lett. **85**, 4606 (2000).

[9] A. Kubetzka, M. Bode, O. Pietzsch, and R. Wiesendanger, Phys. Rev. Lett. **88**, 057201 (2002).

[10] A. Kubetzka, O. Pietzsch, M. Bode, and R. Wiesendanger, Phys. Rev. B. **88**, R020401 (2003).

[11] S.N. Okuno, T. Kishiand, and K. Tanaka, Phys. Rev. Lett. **88**, 066803 (2002).

[12] E.Y. Vedmedenko, A. Kubetzka, K.V. Bergmann, O. Pietzsch, M. Bode, J. Kirschner, H.P. Oepen, and R. Wiesendanger, Phys. Rev. Lett. **92**, 077207 (2004).

[13] T.K. Yamada, M.M.J. Bischoff, G.M.M. Heijnen, T. Mizoguchi, and H.V. Kempen, Phys. Rev. Lett. **90**, 056803 (2003).

[14] H.Q. Yang, A.R. Smith, M. Prikhodko, W.R.L. Lambrecht, Phys. Rev. Lett. **89**, 226101 (2002).

[15] A.R. Smith, R. Yang, H. Yang, W.R.L. Lambrecht, A. Dick, and J. Neugebauer, Surf. Sci. **561(2-3)**, 154 (2004).

[16] D. Wortmann, S. Heinze, Ph. Kurz, G. Bihlmayer, and S. Blügel, Phys. Rev. Lett. **86**, 4132 (2001).

[17] C. L. Fu and A. J. Freeman, Phys. Rev. B **33**, 1755 (1986).

[18] S. Blugel, D. Pescia, and P. H. Dederichs, Phys. Rev. B **39**, 1392 (1989).

[19] M. Bode, M. Getzlaff, and R. Wiesendanger, Phys. Rev. Lett. **81**, 4256 (1998).

[20] R. Wiesendanger, M. Bode, A. Kubetzka, O. Pietzsch, M. Morgenstern, A. Wachowiak, and J. Wiebe, J. Mag. Mag. Mat. **272**, 2115 (2004).

[21] M. Bode, M. Hennefarth, D. Haude, M. Getzlaff, and R. Wiesendanger, Surf. Sci. **432**, 8 (1999).

[22] G.W. Wiener, J.A. Berger, J. Met., **7**, 360 (1955).

[23] F. Lihl, P.Ettmayer, A. Kutzelnigg, Z. Metallk. **53**, 715 (1962).

[24] W.J. Takei, R. R. Heikes, and G. Shirane, Phys. Rev. **125**, 1893 (1962).

[25] M. Mekata, J. Phys. Soc. Jpn., **17**, 796 (1962); M. Mekata, J.Haruna, H. Takei, J. Phys. Soc. Jpn., **25**, 234 (1968).

[26] N. Otsuka, Y. Hanawa, and S. Nagakura, Phys. Stat. Sol. (a), **43**, K127 (1977).

[27] H. Jacobs and C Stuve, J. Less Common Metals, **96**, 323, (1984).

[28] G. Kreiner, and H. Jacobs, J. Alloys and compounds **183**, 345 (1992).

[29] M. Tabuchi, M. Takahashi, and F. Kanamaru, J. Alloys and Compounds **210:(1-2)**, 143 (1994).

[30] K. Suzuki, T. Kaneko, H. Yoshida, Y. Obi, H. Fujimori, H. Morita, J. Alloys and Compounds **306**, 66 (2000).

[31] A. Leineweber, R. Niewa, H. Jacobs, and W. Kockelmann, J. Materials Chemistry **10:(12)**, 2827 (2000).

[32] T. Dietl, H. Ohno, F. Matsukura, J. Cibert, D. Ferrand, Science **287**, 1019 (2000).

[33] H. Yang, H. Al-Brithen, A.R. Smith, J.A. Borchers, R.L. Cappelletti, and M.D. Vaudin, Appl.

Phys. Lett. **78**, 3860 (2001).

[34] H.Q. Yang, H. Al-Brithen, A.R. Smith, E. Trifan, and D.C. Ingram, J. Appl. Phys. **91(3)**, 1053 (2002).

[35] H.Q. Yang, R. Yang, A.R. Smith, and W.R.L. Lambrecht, Surf. Sci. **548**, 117 (2003).

[36] W.R.L. Lambrecht, M. Prikhodko, and M.S. Miao, Phys. Rev. B **68(17)**, 174411 (2003).

[37] A.R. Smith, R. Yang, H.Q. Yang, A. Dick, J. Neugebauer, W.R.L. Lambrecht, Microscopy Res. and Tech. **66(2-3)**, 72 (2005).

[38] J. Tersoff and D.R. Hamann, Phys. Rev. Lett. **50(25)**, 1998 (1983) and Phys. Rev. B **31**, 805 (1985).

[39] R. Yang, H.Q. Yang, A.R. Smith, A. Dick, and J. Neugebauer, to be published.

[40] G.A. Mulhollan, R.L. Fink, J.L. Erskine, and G.K. Walters, Phys. Rev. B **43**, 13645 (1991).

[41] J. Chen and J.L. Erskine, Phys. Rev. Lett. **68**, 1212 (1992).

[42] R. Wu and A.J. Freeman, Phys. Rev. B **45**, R7532 (1992).

[43] A. Kubetzka, P. Ferriani, M. Bode, S. Heinze, G. Bihlmayer, K. von Bergmann, O. Pietzsch, S. Blügel, and R. Wiesendanger, Phys. Rev. Lett. **94**, 087204 (2005).

[44] K. von Bergmann, M. Bode, A. Kubetzka, O. Pietzsch, and R. Wiesendanger, Micr. Res. and Tech. **66**, 61 (2005).

[45] K. Mukasa, H. Hasegawa, Y. Tazuke, K. Sueoka, M. Sasaki, and K. Hayakawa, Jap. J. Appl. Phys. **33**, 2692 (1994).

[46] H. Ness and F. Gautier, Phys. Rev. B **52**, 7352 (1995).

[47] K. Nakamura, H. Hasegawa, T. Oguchi, K. Sueoka, K. Hayakawa, and K. Mukasa, Phys. Rev. B **56**, 3218 (1997); K. Nakamura, T. Oguchi, H. Hasegawa, K. Sueoka, K. Hayakawa, and K. Mukasa, Appl. Surf. Sci. **140**, 366 (1999).

[48] A.S. Foster and A.L. Shluger, Surf. Sci. **490**, 211 (2001).

[49] H. Hosoi, K. Sueoka, and K. Mukasa, Nanotechnology **15**, 505 (2004).

[50] K. Sueoka, A. Subagyo, H. Hosoi, and K. Mukasa, Nanotechnology **15**, S691 (2004).

[51] M. Bammerlin, R. Lüthi, E. Meyer, A. Baratoff, J. Lü, M. Guggisberg, C. Gerber, L. Howard, and H.-J. Güntherodt, Probe Microsc. **1**, 3 (1997).

[52] S. Ciraci, A. Baratoff, and I.P. Batra, Phys. Rev. B **41**, 2763 (1990).

[53] M.R. Castell, S.L. Dudarev, G.A.D. Briggs, and A.P. Sutton, Phys. Rev. B **59**, 7342 (1999).

[54] L.N. Kantrovich, A.L. Shluger, and A.M. Stoneham, Phys. Rev. B **63**, 184111 (2001).

[55] H. Momida and T. Oguchi, Surf. Sci. **590**, 42 (2005).

[56] N. Berdunov, S. Murphy, G. Mariotto, and I.V. Shvets, Phys. Rev. Lett. **93(5)**, 057201 (2004).

[57] I.V. Shvets, N. Berdunov, G. Mariotto, and S. Murphy, Europhy. Lett. **63**, 867 (2003).

[58] S. Murphy, S.F. Ceballos, G. Mariotto, N. Berdunov, K. Jordan, I.V. Shvets, and Y.M. Mukovskii, Microsc. Res. and Techn. **66**, 85 (2005).

[59] J.S. Kasper and J.S. Kouvel, J. Phys. Chem. Sol. **11**, 231 (1959).

[60] W.B. Pearson, K. Brun, A. Kjekshus, Acta Chem. Scand. **19**, 477 (1965).

[61] L. Pál, E. Krén, G. Kádár, P. Szabó, T. Tarnóczi, J. Appl. Phys. **39**, 538 (1968).

[62] S.F. Ceballos, G. Mariotto, S. Murphy, and I.V. Shvets, Surf. Sci. **523**, 131 (2003).

[63] N. Berdunov, S. Murphy, G. Mariotto, I.V. Shvets, and Y.M. Mykovskiy, J. Appl. Phys. **95(11)**, 6891 (2004).

[64] E.Y. Tsymbal, O.N. Mryasov, and P.R. LeClaire, J. Phys. Condens. Matter **15**, R109 (2003).

[65] M. Bode, S. Heinze, A. Kubetzka, O. Pietzsch, M. Hennefarth, M. Getzlaff, R. Wiesendanger, X. Nie, G. Bihlmayer, and S. Bl*ü*gel, Phys. Rev. B **66**, 014425 (2002).

[66] S. Heinze, P. Kurz, D. Wortmann, G. Bihlmayer, and S. Blügel, Appl. Phys. A **75**, 25 (2002).

[67] W.A. Hofer and A.J. Fisher, Surf. Sci. **498**, L65 (2002).

[68] J. Bardeen, Phys. Rev. Lett. **6**, 57 (1961).

[69] W.A. Hofer and A.J. Fisher, J. Mag. and Mag. Mat. **267**, 139 (2003).

[70] W.A. Hofer, A.J. Fisher, R.A. Wolkow, and P. Grütter, Phys. Rev. Lett. **87**, 236104 (2001).